THE JOURNAL OF PHYSICAL CHEMISTRY C

ARTICLE

pubs.acs.org/JPCC

^{29}Si NMR and UV−Raman Investigation of Initial Oligomerization Reaction Pathways in Acid-Catalyzed Silica Sol−Gel Chemistry

Anouschka Depla,[†] David Lesthaeghe,[‡] Titus S. van Erp,[†] Alexander Aerts,[†] Kristof Houthoofd,[†] Fengtao Fan,[§] Can Li,[§] Veronique Van Speybroeck,[‡] Michel Waroquier,[‡] Christine E. A. Kirschhock,[†] and Johan A. Martens*[,†]

[†]Center for Surface Chemistry and Catalysis, K.U. Leuven, Heverlee, Belgium

[‡]Center for Molecular Modeling, Ghent University, Zwijnaarde, Belgium

[§]Science, Engineering and Technology Group, and State Key Laboratory of Catalysis, Dalian Institute of Chemical Physics, Chinese Academy of Sciences, Dalian, China

Supporting Information

ABSTRACT: The initial molecular steps of the acid-catalyzed silica sol−gel process departing from tetraethylorthosilicate (TEOS) were investigated by in situ ^{29}Si NMR and UV−Raman spectroscopy. The use of a substoichiometric H_2O:TEOS molar ratio (*r*-value 0.2−1.2) slowed the silicate oligomerization reaction and allowed unraveling the initial steps of silica condensation. Molecular modeling confirmed Raman signal and ^{29}Si NMR shift assignment. A comprehensive listing of all Raman and ^{29}Si NMR assignments is provided, including unique Raman assignments of cyclosilicates and the linear tetramer. The combination of experiment and modeling allowed an analysis of the reaction kinetics. The derived kinetic model and the experimental observation both revealed that the H_2O:TEOS molar ratio had a strong influence on the reaction kinetics but not on the reaction pathways. The multianalytical approach led to development of an oligomerization scheme. As dominant oligomerizations, chain growth, cyclodimerization, and branching were identified. Under the investigated conditions, chains did not grow longer than pentamer, and ring sizes were limited to 6-rings. Chains of 4 Si atoms and 4-rings were abundant species. Branched rings and chains were formed by attachment of dimers and trimers. Gelation proceeded from branched 4-rings and branched chains with limited hydroxyl functionalities.

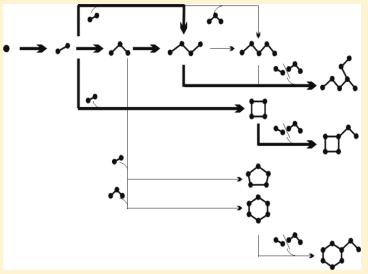

INTRODUCTION

Sol−gel techniques are applied in industry for manufacturing a variety of silica materials including sols, gels, porous glasses, films, and fibers.[1−4] Silica sol−gel processing refers to hydrolytic polycondensation of a silicon source in the presence of solvent and homogeneous catalyst. Careful control of the sol and its transformation to gel allows synthesis of a wide variety of silica materials with specific properties depending on synthesis conditions. Each step in the synthesis process affects the final material properties.[5−7] Crucial parameters of the silica sol−gel processes are the water:alkoxide molar hydrolysis ratio or *r*-value, the pH, and the nature of the alkoxide.[5,8−17] In general terms, homogeneous acid catalysts direct silica polymerization toward linear polymers and materials having low fractal dimension, while basic catalysts generally favor formation of tridimensional highly branched silicate networks.[8,15]

Raman spectroscopy and ^{29}Si NMR are frequently used for investigation of silica polymerization.[13,14,18−27] In alkaline media, silicon displays a complex polyanion chemistry.[21,28−30] Identification of a large number of polyanion species in alkaline media has been achieved through a combination of NMR spectroscopy and molecular modeling.[28,31,32] In recent years, Raman spectroscopy emerged as a powerful tool for the characterization of silicate precursor molecules in zeolite synthesis.[33−38] Zeolite framework building units like ring structures with 4−8 Si atoms can be identified based on a breathing vibration mode in the low-frequency region, which shifts depending on ring size.[37,39−45] Ring vibrations are highly sensitive to the incorporation of Al atoms, the interaction with cations, and solvation.[46−53] Compared to former investigations of zeolites using IR− or Vis−Raman, the application of UV−Raman spectroscopy presents significant improvement with respect to signal-to-noise ratio and avoids fluorescence interference. The possibility to analyze silica oligomerization processes without spectral interference of the aqueous solution is an important advantage of UV−Raman spectroscopy. Detection and identification in aqueous solution of small cyclosilicates, branched chains, and higher oligomers including double rings and other cagelike structures have been reported.[33,36,54−56]

Received: October 15, 2010
Revised: January 3, 2011
Published: February 10, 2011

Table 1. Overview of Samples

sample code	r_n-value	r-value	TEOS (mL)	EtOH (mL)	H_2SO_4 (mL)	H_2O (mL)	TEOS:H_2O:EtOH:H_2SO_4 molar ratio
R-0.2	0.02	0.2	10.824	8.711	0.465	----	1:0.2:3.08:0.35
R-0.7	0.5	0.7	10.602	8.532	0.455	0.411	1:0.7:3.08:0.35
R-1.2	1	1.2	10.380	8.353	0.446	0.822	1:1.2:3.08:0.35

In contrast to alkaline media, literature on silica speciation in acid-catalyzed sol−gel chemistry is more limited. The present descriptions of the possible reaction pathways in acidic media even are ambiguous. Several authors adhere to a model of linear chain growth,[8,14,19] while others reported cyclization reactions competing with chain extension.[57,58] Theoretical predictions of gelation times were in better agreement with experimental data when cyclization was accounted for.[57,23] Depending on the alkoxide, the contribution of cyclization was found to increase with increasing r-value.[57] Pentamers and longer oligomers, grown in acidic medium, were found to contain branching of their silicate chain.[59] Mulder and Damen investigated acid-catalyzed TEOS hydrolysis and condensation in the presence of substoichiometric water quantities using Vis−Raman spectroscopy.[14] At an experimentally determined r-value of 1, those authors observed the formation of hydrolyzed monomer, linear chains up to tetramer, and branched species. The reduction in molecular mass by hydrolysis of ethoxide substituents causing vibrations to shift to higher wavenumbers turned out as a convenient guide for the assignment of Raman signals.[13,14]

Here, we report an investigation of silica polycondensation under strongly acidic conditions at low r-values by in situ ^{29}Si NMR and UV−Raman. Low hydrolysis ratios offer the advantage of limited hydrolysis and slow reaction kinetics allowing investigation with ^{29}Si NMR. The combination of the two experimental techniques with molecular modeling allowed identification of the majority of silicate species. This led to derivation of a model of the reaction kinetics in full agreement with all experimental observations. With the kinetic model, the complete oligomerization reaction network could be established, which eventually determines the connectivity and properties of the final silica gel. Experimental evidence showed that the mechanism is rather insensitive toward water content, temperature, and type of mineral acid catalyst. The silica gel materials obtained under the here described conditions are microporous with narrow monomodal pore size distribution and have been reported to be suitable for controlled release of drug molecules and antiseptic agents.[60−64]

EXPERIMENTAL SECTION

The sol−gel synthesis was performed at room temperature while continuously stirring with a magnetic bar. Typically, TEOS (Acros, 98%) was dissolved in ethanol (VWR, absolute grade, 99.9%). Concentrated H_2SO_4 (98%, Fisher) and, optionally, water were added dropwise in this order under continuous stirring. The molar ratio of TEOS:EtOH:H_2SO_4 was 1:3.08:0.35. The nominal molar H_2O:TEOS ratio (r_n-value) was 0.02, 0.5, or 1. The sample preparation was performed in open air. Afterward, the samples were either sealed in polypropylene bottles (20 mL) for sample aging or transferred into the NMR tube and sealed during ^{29}Si NMR analysis. The possibility that before sealing the samples some water may have been absorbed from ambient, therewith altering the r_n-value, was accounted for. The true r-value was determined using the Q^i distribution of Si atoms determined by ^{29}Si NMR sequences. Each hydrolysis of an ethoxide group resulting in either a siloxane bond or a hydroxyl function requires exactly one water molecule. Thus, the number of siloxane bonds plus the number of hydroxyl functions corresponds directly to the number of consumed water molecules. Assuming all water in the sample was converted, the true r-value equals eq 1

$$r = \frac{1}{2}\sum_{i=1}^{4} iQ^i + \sum_{i=1}^{4} Q_h^i \qquad (1)$$

In eq 1, subscript h refers to hydrolyzed species. The r-value for the samples with an r_n-value of 0.02, 0.5, and 1.0 was 0.2, 0.7, and 1.2, respectively. The significantly higher values reveal the hygroscopic nature of these samples, while stability of the final experimental r-values over days to weeks in sealed samples indicated all water indeed was consumed. During the remainder of the article, the true r-values will be used. The sample code names and chemical compositions for the synthesis of 20 mL batches of the respective samples are listed in Table 1.

Raman spectra were recorded using excitation by a Coherent Innova 300C MotoFred laser. The laser beam was guided to the sample by dielectric broadband mirrors and a TGS1 type lens, both of a UV grade fused silica substrate material. The Raman signal was collected in backscattering geometry. The scattering was guided toward an Al-coated parabolic mirror, which focused the signal onto the entrance of a Roper Scientific Trivista TR557 A&S triple-stage spectrometer. Within the respective stages, a 900−900−3600 grooves/mm grating combination spread the Raman signal. Detection occurred with a liquid nitrogen cooled back-illuminated CCD camera (Princeton Instruments). The optical path was home-built. Samples were excited with a 244 nm beamline at an output power of 10 mW. During analysis of the silicate solution in shallow cylindrical holders, a minimal exposure time of 100 s was respected, and rotation was applied to minimize local heating. All spectra represent an average of four accumulations, each time on a fresh sample. After recording, spectra were normalized for intensity and calibrated for possible instrumental frequency shifts. A smoothing by a Savitzky−Golay algorithm with a filter coefficient of 5 was applied. Intensity normalization was based on the 1455 cm^{-1} vibration, assigned to the asymmetrical C−H bending of ethoxide groups of both TEOS and EtOH. As a guide for the eye the spectra were normalized on this concentration of ethoxide groups. PTFE was used as a shift reference. Several UV−Raman spectra at enhanced excitation power (30 mW) were acquired on a Raman spectrometer at the Chinese State Key Laboratory of Catalysis.[56]

^{29}Si NMR spectra of samples R-0.2 and R-1.2 were recorded on a Bruker AMX300 spectrometer (7.0 T). Experimental conditions cover a recycle delay of 20 s and a pulse length of 12.0 μs. Immediately after mixing, sample volumes of 2 mL were transferred into 10 mm PTFE tubes and spun at a frequency of 16 Hz. An internal chemical shift and lock reference served tetramethylsilane and acetone-d_6, respectively. The numbers of accumulations for sample R-0.2 and R-1.2 were 17 577 and

dx.doi.org/10.1021/jp109901v |J. Phys. Chem. C 2011, 115, 3562–3571

13 306. At regular times, the accumulated signal was stored. Si atom distributions were derived from the spectra by fitting individual signals with Voigt-type peak functions.

The ^{29}Si NMR spectra of sample R-0.7 were recorded on a Bruker Avance II^{+} 600 spectrometer (14.1 T). Samples (3 mL) were transferred into 10 mm quartz tubes. The spinning frequency was 16 Hz. Experimental conditions comprised a recycle delay of 80 s, a pulse length of 12.0 μs, and a power level at −1.50 dB, corresponding to $\pi/2$-pulses. Tetramethylsilane served as the external chemical shift reference. Measurements were performed without lock, under isothermal conditions at 298 K. Shimming was performed on a solution of TMS−salt (trimethylsilyl−propane sulfonic acid, Merck) in 3 mL of D_2O. Each acquisition in the time sequence represented an accumulation of 28 scans.

THEORETICAL SECTION

For an adequate determination, Raman vibrational frequencies, Raman intensities,[65] and ^{29}Si NMR chemical shifts[66] were calculated using the program Gaussian03.[67] Quantum chemical methods are mandatory for adequate determination of Raman intensity as opposed to IR spectra where classical molecular dynamic methods provide sufficiently accurate results.[68] All chain structures from monomer up to hexamer and five cyclosilicates (a 3-, 4-, 5-, and 6-ring and a double-4-ring) were optimized in vacuo at the B3LYP/6-31+g(d) level of theory,[69] a level of theory similar to that used for previous studies on silica oligomerization.[70] At this particular level, it is known that one may easily underrate vibrational frequencies with a scale factor between 0.9636 and 1.0000, dominated by high and low frequencies, respectively.[71] With the initial monomer as a benchmark, we obtained a scale factor of 0.99, well within the expectations. The model assumes all species fully saturated with ethoxide groups, justified at low molar hydrolysis ratio, and confirmed by NMR analysis of R-0.2. The configurational dependency of the spectra was verified by considering two different conformers for each chain species, both linear and curled up. The maximal variation between any such pair of conformers was ∼20 cm^{-1} with energy differences between the conformers typically smaller than ∼2 kJ mol^{-1}. This value was subsequently adopted as the margin of error for the theoretical Raman shifts. For the ^{29}Si NMR chemical shifts, the shifts were calculated for all silicon atoms of the mentioned structures and their conformers and averaged out over Q^0, Q^1, Q^2 and Q^3. A distinction was made between Q^2 species in chains and Q^2 species in rings. Single-point calculations with a triple-ζ basis set 6-311++g(d,p) were performed on B3LYP/6-31+g(d) optimized geometries for the ^{29}Si NMR signals. The Q^0 signal of TEOS monomer served as reference for the theoretical ^{29}Si chemical shifts, leading to a scale factor of 0.9463. The Supporting Information contains Cartesian coordinates for all optimized structures (see Molecular modeling in Supporting Information).

RESULTS AND DISCUSSION

Silica Oligomer Speciation of TEOS Condensation at Low *r*-Value in Acidic Conditions. The evolution of oligomeric species at low *r*-values in strongly acidic conditions was investigated by in situ ^{29}Si NMR and UV−Raman. Under such conditions hydrolysis was limited and reaction kinetics were slow and all samples homogeneous, which were ideal circumstances to collect high-quality spectra. The condensations, departing from three different *r*-values (R-0.2, R-0.7, and R-1.2), were monitored. The experimentally lowest achievable *r*-value of 0.2 was imposed by the intrinsic water content of concentrated sulfuric acid. With increasing *r*-value the NMR spectra gained complexity so that the set of samples allowed identification of the majority of formed silicate species. For the Raman spectra, the used UV-excitation source of 244 nm was mandatory to achieve high signal-to-noise ratios, compared to Raman applications with a VIS-laser source. A UV source also circumvents possible interference of fluorescence.[33,36,72] Full and consistent assignment of all observed ^{29}Si NMR and Raman spectroscopic signals successfully was achieved through combination of experiment with molecular modeling using the B3LYP density functional (as described in the Experimental Section).

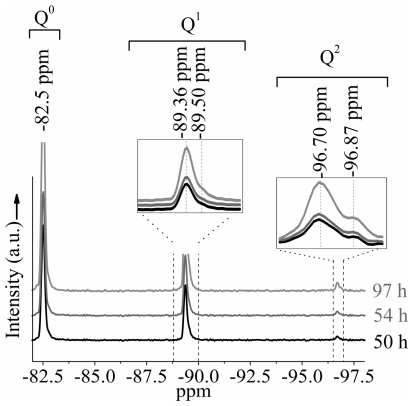

Figure 1. ^{29}Si NMR of the initial stages in the condensation process of the R-0.2 sample.

Accumulated ^{29}Si NMR spectra recorded during the evolution of R-0.2 (Figure 1) revealed the presence of a monomer (Q^0, δ = −82.5 ppm), dimer (Q^1, δ = −89.36 ppm), and two types of Q^2 silicon atoms connected to two silicate units. The latter were assigned to linear trimer (δ = −96.70 ppm) and tetramer (δ = −96.87 ppm).[10,58] The signals of the Si atoms terminating these chains, Q^1, were observed at δ = −89.5 ppm, clearly different from the Q^1 signal of the dimer. This interpretation of the ^{29}Si NMR spectroscopic signature is in full accordance with the literature and confirmed by molecular modeling (Table 2). No higher degrees of condensation were detected. Most surprisingly, no indication for the presence of 3- or 4-rings was observed. Such species might form by ring closure of the observed linear trimer and tetramer. Possible explanations for the absence of such cycles might be the presence of bulky ethoxy groups at terminating silica which prevent suitable conformations allowing ring closure and the low probability of the hydrolysis of the chains present in only very low concentrations compared to the monomer.

This assignment of all species present in R-0.2 provided an important verification of the validity of the applied combination of ab initio calculations with Raman analysis. The Raman signatures of the monomer (∼655 cm^{-1}), dimer (∼600 cm^{-1}), and linear trimer (∼580 cm^{-1}) were readily identified. The signal around 600 cm^{-1} comprised both dimer (∼594 cm^{-1}) and end groups of chains (∼602 cm^{-1}).[14,19] The additional vibrations at ∼430 and ∼882 cm^{-1} were caused by ethanol as verified by reference measurements and the literature.[14,22] However, an additional signal at ∼565 cm^{-1} could not immediately

Table 2. Experimental and Theoretical ^{29}Si NMR Chemical Shifts

			experimental ^{29}Si NMR signal (ppm)		
Q^i region	theoretical region (ppm)	species	R-0.2	R-0.7	R-1.2
Q^0	−82.1;-82.9	monomer	−82.50	−82.50	-----
Q^1	−86.8;-92.7				
		dimer	−89.36	−89.36	−89.36
		end group	−89.50	−89.53 *and* −89.75	−89.53
Q^2 chains	−96.7;-103.9				
		trimer	−96.70	−96.72	−96.72
		tetramer	−96.87	−96.89	−96.89
		pentamer	-----	−97.10	−97.10
Q^2 *n*-rings	−94.2;-100.4	($n \geq 4$)			
	−86.0;-88.4	($n = 3$)			
		3-ring	-----	−88.4	−88.4
		4-ring	-----	−95.69	−95.69
		5-ring	-----	−95.94	−95.94
		6-ring	-----	−96.10	−96.10
Q^3	−103.5;-105.8				
		branched chain	-----	−103.3	−103.3
		branched ring	-----	−102	−102
		Q^i region for 1 time hydrolyzed species			
Q^0 hydr.		monomer	-----	−79.59	-----
Q^1 hydr.		dimer *and* end group	-----	−86.82 *and* −86.88	−86.82
Q^2 hydr. chain		chain	-----	−94.50	−94.50
Q^2 hydr. ring		ring	-----	−93.34	−93.34
Q^3 hydr. chain		branched chain	-----	-----	−100.6

be identified. Assignment to sulfuric acid was discarded based on reference measurements of concentrated acid, which showed intense signals at ∼920, ∼1054, and ∼1145 cm^{-1} and broad signals at ∼420 and ∼560 cm^{-1}. In the R-0.2 spectrum (Figure 2), the sulfuric acid signals coincided with intense signals of ethanol and TEOS. To fully exclude that sulfuric acid caused the signal at 565 cm^{-1}, it was substituted by hydrochloric acid (see Figure 1 of Supporting Information) at an experimentally determined *r*-value of 1.2. A similar Raman signal at ∼560 cm^{-1} was observed. Clearly, this signal originated from a silica-oligomer. Reflecting on the species identified by ^{29}Si NMR (Figure 1), the ∼565 cm^{-1} vibration had to relate to the linear tetramer, although the literature reports this vibration at lower wavenumbers (∼545 cm^{-1}).[14,19] Molecular modeling could confirm this assignment (Table 3). The computer model accounted for the "open" and "closed" configurations of all chains, as visualized for the tetramer in Figure 3. The isolated Raman active band represents a global stretching vibration of the open tetramer, which converts into a general ring breathing vibration as the chain curls into the closed tetramer. These particular vibrations are symmetry forbidden and inactive in IR spectroscopy. Taking both conformers into account, molecular modeling confirms tetramer vibrations to occur in the region 540−560 cm^{-1}. The broad Raman signature occurring around 800 cm^{-1} comprises the asymmetrical Si−O stretch (795 cm^{-1}) and the CH_2-rocking (810 cm^{-1}).[14,22] The 960 cm^{-1} vibration is attributed to the CH_3-rocking. The Raman band occurring at 933 cm^{-1} corresponds to the C−C symmetrical stretch of fully ethoxide terminated monomers.[14,73] Raman bands at 295 and 340 cm^{-1}, based on analysis of Raman spectra of silica oligomerizations departing from

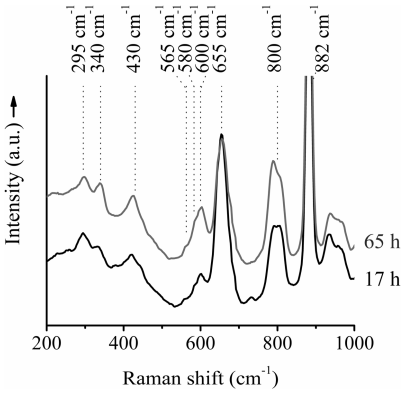

Figure 2. UV−Raman spectra after 17 and 65 h of the condensation process of the R-0.2 sample.

different acid catalysts, were found to be dependent on the catalyst and were less relevant to the present analysis of oligomerization pathways.

Limited by the low water content, R-0.2 evolved very slowly. After 96 h, the longest chains were tetramers. The *r*-value was elevated to 0.7 to experimentally access more condensed oligomers. The increased complexity of the system called for an increased spectral resolution for the ^{29}Si NMR experiments. ^{29}Si NMR spectra of the R-0.7 sample were recorded on a Bruker Avance II$^+$ 600 spectrometer offering the necessary resolving power to distinguish between the different Q^i environments (Figure 4). Next to the signals of chains up to tetramer observed in R-0.2, the presence of a broad signal at $\delta \sim -97.10$ ppm

dx.doi.org/10.1021/jp109901v |*J. Phys. Chem. C* 2011, 115, 3562–3571

Table 3. Experimental and Theoretical Raman Shifts

species	experimental shift (cm^{-1})	theoretical shift region (cm^{-1})
monomer	655	645−665
dimer (+end groups)	600	585−605
trimer	580	560−580
tetramer	565	540−560
pentamer	----	535−555
3-ring	----	580−600
4-ring	540	535−555
5-ring	----	530−550
6-ring	----	540−560

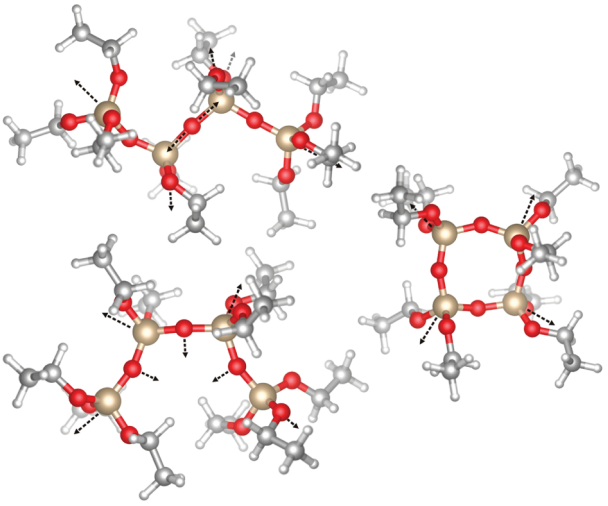

Figure 3. Different conformers of the tetramer species: open configuration (top left), closed configuration (bottom left), and 4-ring (right). The Raman active global chain stretching vibration converts into a general ring breathing vibration as the chain curls up.

revealed the formation of increasingly longer chains. Due to the increased hydrolysis ratio in R-0.7, cyclosilicates, especially 4-rings (Q^2, δ = −95.69 ppm), 5-rings (Q^2, δ = −95.94 ppm), and 6-rings (Q^2, δ = −96.10 ppm), next to small quantities of 3-rings (δ = −88.4 ppm), emerged. The occurrence of a cyclic trimer at low pH and similar *r*-values has been reported before.[59]

R-0.7 also contained silica connected to three further silicate units (Q^3). This unmistakably proved the presence of branching of chains (δ = ∼ −103.3 ppm) and rings (δ = ∼ −102 ppm). Computation of the theoretical chemical shifts for every observed silicon environment confirmed these assignments (Table 2). While in R-0.2 all silicon atoms carried ethoxide groups, in R-0.7 some silicate species with a hydrolyzed group were also detected: monomer (Q^0, δ = −79.59 ppm), dimer (Q^1, δ = −86.82 ppm), chains (Q^1, δ = −86.88 ppm and Q^2, δ = −94.50 ppm), and rings (Q^2, δ = −93.34 ppm). The increased concentration of hydroxide groups in the silicate species clearly was responsible for the observed formation of rings and branchings.

Like the spectra of R-0.2, UV−Raman spectra of R-0.7 (Figure 5) indicated the presence of monomer, dimer, linear trimer, and tetramer. In this sample, a signal around ∼570 cm^{-1}

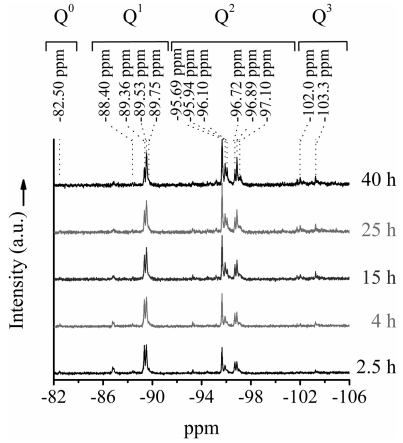

Figure 4. ^{29}Si NMR spectra of the condensation process of the R-0.7 sample at the indicated times.

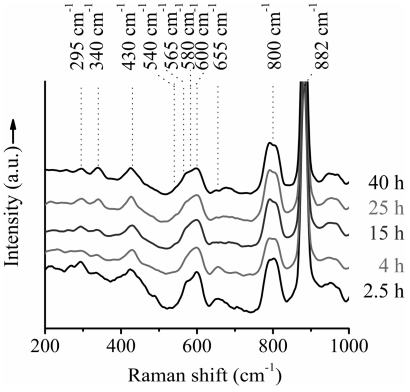

Figure 5. UV−Raman spectra of the initial stages in the condensation process of R-0.7.

was present and correspondingly attributed to an overlap of signals of trimer (580 cm^{-1}) and tetramer chains (565 cm^{-1}). A similar overlap of Raman signals of trimer and tetramer was observed in the R-0.2 sample after longer reaction times of 140 h (see Figure 2 of Supporting Information). A new Raman signal at ∼540 cm^{-1} emerged after 4 h as a shoulder of the 565 cm^{-1} band. Theoretically the breathing vibration mode of 4-rings was expected in the 535−555 cm^{-1} region (Table 3). According to ^{29}Si NMR, 4-rings emerged exactly during the same period as the 540 cm^{-1} Raman signal (Figure 4). Therefore, the intensity around ∼540 cm^{-1} at least partially corresponded to the presence of 4-rings. According to the molecular models, discrimination between Raman signatures of linear tetramer and longer chains was expected to be difficult (Table 3). The Raman band of the pentamer was expected around 535−555 cm^{-1}, overlapping not only with the tetramer but also with the 4-ring region (Table 3). Similarly, distinction between 4- and larger rings by Raman spectroscopy theoretically also was to be expected ambiguous (Table 3). On the basis of these theoretical results, the observed intensity at ∼540 cm^{-1} finally was assumed to contain contributions of minor populations of 5- and 6-rings and longer chains, next to the much more abundant 4-rings. This was found to be directly reflected in the broad nature of the observed band.

In the ^{29}Si NMR spectra, the intensity of the Q^2 signal assigned to 4-rings (δ = −95.69 ppm) was high (Figure 4), while in the

dx.doi.org/10.1021/jp109901v |*J. Phys. Chem. C* 2011, 115, 3562–3571

UV−Raman spectra, the Raman signature at 540 cm^{-1} assigned to 4-rings was rather weak (Figure 5), which might seem contradictory. Raman signal intensity relies not only on the concentration of the species but also on other parameters like the Raman cross section of each particular vibration, which for an isolated ring can be low. In ^{29}Si NMR the signal is related to the number of atoms, and 4-rings containing four Q^2 silicon atoms each generate an intense signal. In addition, in the Raman spectra, the signal assigned to 4-rings was broadened and contained some contribution of larger rings as well (Figure 5).

A further increase in the *r*-value to 1.2 led to some interesting observations. Despite the higher degree of hydrolysis, the ^{29}Si NMR spectroscopic signature of R-1.2 revealed analogous species compared to R-0.7 (see Figure 3 of Supporting Information). Even at this elevated *r*-value, the formation of chains still remained favored over cyclization. More remarkably, the oligomers did not grow larger than in R-0.7. Linear chain growth still was limited to pentamer (Q^2, δ = −97.10 ppm), and the ring sizes, like before, were limited to 6-rings. Only during a short period after mixing of the reagents, low concentrations of 3-rings were observed (Q^2, δ = −88.4 ppm). Compared to R0.7, the branching on rings (Q^3, δ = −102 ppm) and chains (Q^3, δ = −103.3 ppm) gained importance, and also hydrolysis of ethoxide groups was more pronounced, as expected for a higher hydrolysis ratio. A listing of ^{29}Si NMR signals present in R-1.2 is provided in Table 2.

The first UV−Raman spectra of R-1.2 fully confirmed the presence of chains and rings. (See Figure 7 of Supporting Information.) Similar to the R-0.7 sample, signals of linear trimer and tetramer (580 and 565 cm^{-1}) overlapped in the first stages of R-1.2 evolution. Around 20 h, the 565 cm^{-1} vibration of tetramer became dominant. Signals of dimer and end groups (∼600 cm^{-1}) were discernible together with the 4-ring vibration (540 cm^{-1}). All monomers were consumed before the first recording, similar to the observations by ^{29}Si NMR. In later stages of R-1.2 oligomerization, all Raman signals broadened. This phenomenon was ascribed to the increasing branching of both chains and rings, also detected via ^{29}Si NMR (see Figure 3 of Supporting Information). A broadening of the ∼540 cm^{-1} signal was ascribed to the additional formation of 5- and 6-rings evidenced by ^{29}Si NMR. As mentioned before, theory indicated Raman intensities of small cycles all appear in the same region. Finally, in the last spectrum (500 h) the Raman signals fully merged to a broadened signature around ∼530 cm^{-1}. By now the dimer signal had vanished, and the remaining vibration at 600 cm^{-1} corresponded to end groups of chains and branches. This spectral evolution was interpreted as formation of an increasingly branched silicate population which ultimately, after 5−6 weeks, led to gelation.

The above derived identification of silica oligomers implied a quite narrow and well-defined oligomer speciation during hydrolysis and condensation of TEOS in strongly acidic media at low *r*-values. This observation is in huge contrast to the wealth of polyanions reported in the literature for sol−gel synthesis in alkaline media.[21,28−32] The strong acidity and low molar hydrolysis ratio apparently restricted the speciation to short linear chains and small cyclosilicates, with abundant trimeric chains in R-0.2 and tetramers and 4-rings at a slightly higher *r*-value in R-0.7. An increased *r*-value of 1.2 only resulted in more pronounced contributions of branching, while the formation of chains still remained favored over cyclization. The final oligomer distribution before gelation was characterized by the strongly dominating presence of branched 4-rings and branched chains

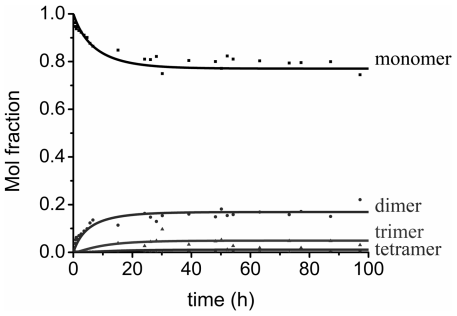

Figure 6. Evolution of molar fractions of monomer and oligomers in the R-0.2 sample. The solid lines represent the fitted oligomerization model.

with limited hydroxyl functionalities. The described accurate assignment of all spectroscopic signals was only possible by the combination of the spectroscopic techniques with profound molecular modeling.

Reaction Scheme of TEOS at Low *r*-Value and Acidic Conditions. With the accurate identification of all oligomeric species evolving from a single monomeric TEOS population, derivation of a model of the oligomerization pathways and their reaction kinetics was within reach. ^{29}Si NMR allowed accurate determination of relative concentrations of the present oligomeric species. Due to the very slow kinetics at the studied low pH and low water content, acquisition of a time-resolved evolution of the oligomerization was possible. The ^{29}Si NMR data of R-0.2 (Figure 1) revealed that the monomer concentration initially decreased in favor of dimer (Figure 6). Later the concentration of dimer reached a steady concentration, while the monomer continued to be consumed. Trimer together with small amounts of tetramer were formed. The UV−Raman spectra of R-0.2 are shown in Figure 2. In the temporal sequence of spectra, the intensity of the monomer signal decreased, while the signatures of dimers, trimers, and tetramers gained intensity. This trend in the UV−Raman spectra of R-0.2 was in full agreement with the quantitative polymerization scheme suggested by ^{29}Si NMR. Apparently, the experimental protocol ensured a good correlation between samples studied by ^{29}Si NMR and UV−Raman.

The observed evolution of oligomer concentrations pointed at chain elongation by monomer addition, which was translated into a kinetic model (see Kinetic model in Supporting Information). This model accounted for the following reactions

$$m_1 + w \xrightarrow{k_h} m_1^*$$

$$m_1 + m_1^* \xrightarrow{k_2} m_2$$

$$m_2 + m_1^* \xrightarrow{k_3} m_3$$

$$m_3 + m_1^* \xrightarrow{k_4} m_4$$

with *w* being water, m_1, m_2, m_3, and m_4 being monomers, dimers, trimers, and tetramers saturated with ethoxy, and asterisks representing singly hydrolyzed species. Theoretically, we found no significant energetic differences between Q^0 and Q^1 hydrolysis, but statistically the monomers were in great excess of endgroups of chains, so that encounters between chains and water molecules or hydrolyzed monomers occurred only sporadic, if ever. On the basis of this, the kinetic model exclusively

considered hydrolysis of monomers, and hydrolysis of chains was neglected. The validity of this assumption was confirmed by the experimental data where no hydrolyzed species were observed for systems with these extremely low water contents and by the literature.[8]

As the rate-limiting step, the hydrolysis of the monomer TEOS was assumed. This assumption was justified by other authors also reporting this to be the rate-limiting step in silica sol−gel processes at low pH.[11,59] This kinetic model, based on a reaction scheme with stepwise monomer addition, accurately described the experimental observations, as seen from the excellent correlation in Figure 6 (solid lines). The fitted rate constants for hydrolysis and dimer formation were k_h = 0.16 h^{-1} and k_2 = 100 h^{-1}, respectively. Inspection of the mathematical model immediately revealed that the absolute values of k_2, k_3, and k_4 had no influence at all, and only their relative values mattered. The ratios of the rate constants, $\kappa_i = k_i/k_2$, were $\kappa_3 = \kappa_4 = 2.63$, which is to be expected as the experiment revealed chain growth and not branching as the dominant pathway. The kinetic model explicitly contained the amount of water which could be used to verify the chemical composition of the studied samples. An optimum fit with the experimental data was obtained for an *r*-value of ∼0.2, which goes far beyond the amount of water nominally introduced by mixing (H_2O:TEOS ratio of 0.02). This observation confirmed the need and justification to verify the molar hydrolysis ratio experimentally, as outlined in the Experimental Section. Most conveniently, NMR allowed the direct determination of the *r*-value as 0.2. The silicon condensation degree, *p*, is determined from eq 2 with *f* corresponding to the functionality of the monomer, which in the case of TEOS equals 4[74]

$$p = (\sum_{i=1}^{4} iQ^i)/f \qquad (2)$$

The condensation degree was determined to be ∼11%, corresponding to an *r*-value of 0.2 in R-0.2. Considering the exact same value was derived from the kinetic model, it can safely be assumed it described the initial oligomerization pathway correctly. Kelts and Armstrong also observed a condensation degree in excess of the theoretical value based on water content and postulated water uptake from the ambient air.[59] This assumption now can be assumed to be proven.

On the basis of the kinetic model, dimer formation occurred in R-0.2 about 2.6 times slower than chain propagation from dimer to trimer and trimer to tetramer. This was at first a surprising result, but computational studies on a related system of silicate condensation revealed a similar trend.[32,75,76] Different energy barriers for dimerization and chain growth were determined from the removal of the leaving group concluding in siloxane formation. The lower barrier for chain growth was explained by a difference of the solvent structure around the species. An external hydrogen bonded network was assumed to assist in the necessary proton transfer. A similar mechanism could explain preference of chain growth to trimer and tetramer over dimerization in the present system.

The here-developed kinetic model showed for different water concentrations the same fractions of monomer, dimer, trimer, and tetramer, though at different times. Comparison of this kinetic result indicated that irrespective of the initial water content the reaction path remained the same. The *r*-value was found only to determine the rate and termination of the polymerization process. This discovery encouraged the attempt to extrapolate the mechanism of the oligomerization of TEOS toward higher *r*-values and different conditions. The major condition for success of such an extrapolation was whether differing systems indeed evolved in a similar fashion along similar pathways. Only if the derived mechanism of oligomerization could reliably be transferred to other systems, a concise tailoring of synthesis could be within reach. If indeed the sequence of oligomerization and polymerization remained identical, as already suggested by the derived kinetic model, then eventually R-0.2 should reach a state comparable to R-1.2. However, due to the extremely slowed kinetics in R-0.2 a direct comparison at progressed degrees of condensation was unpractical. Still, R-0.2 provided an important clue (see Figure 4 of Supporting Information). Using an increased laser power of 30mW instead of 10 mW, and increasing therewith the temperature in the sample, turned out to accelerate the oligomerization. The same Raman signals assigned to cyclic and linear species observed in samples with higher *r*-values using the 10 mW laser were detected in the R-0.2 sample under stronger radiation. After 94 h, a Raman spectrum almost identical to a spectrum of R-1.2 after 20 h could be obtained in this way. This suggested the oligomerization scheme of concentrated systems under investigation to be rather independent of not only the *r*-value but also temperature. A UV−Raman sequence of TEOS condensation at an r_n-value of 2 validated the oligomerization scheme even up to an r_n-value of 2. The only remaining issue for a generalization of a polymerization scheme was the use of sulfuric acid instead of HCl which typically is the reagent used during silica polymerization at low pH.[60−62] However, with the significant water content of concentrated HCl of ca. 37%, the lowest achievable *r*-value is 1.2. The silica oligomerizations catalyzed by hydrochloric and sulfuric acid were compared using UV−Raman spectroscopy (H_2SO_4-*r*-value of 1.2 and HCl-r_n-value of 1.2). On the basis of the Raman spectra, the use of HCl instead of H_2SO_4 did not alter the oligomerization process (see Figure 1 of Supporting Information).

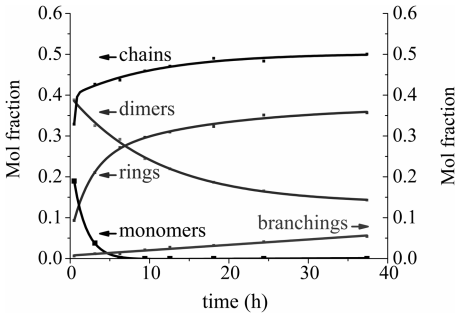

Figure 7. Evolution of mole fractions of monomer and different types of oligomers in the R-0.7 sample (derived from Q^0, Q^1, and Q^2 signals in ^{29}Si NMR) and fraction of branching expressed as the fraction of Q^3 in totality of silicon atoms. Lines are meant to guide the eye.

With these, admittedly rather qualitative, indications that a general oligomerization mechanism holds true under a broad range of conditions, a more detailed analysis of the formation mechanism and sequence of silicate oligomers and networks was derived based on quantitative analysis of species observed in R-0.7 and R-1.2.

Compared to R-0.2, at the higher *r*-value of 0.7, ^{29}Si NMR and the UV−Raman spectra of the sol−gel synthesis revealed the presence of an increased number of species at earlier times, among those cyclic and branched silicates. An increased resolution of the ^{29}Si NMR spectra, achieved at 600 MHz, was mandatory for accurate molar quantification of all linear and

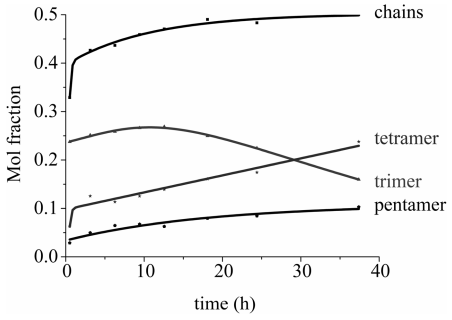

Figure 8. Detail of Figure 7 showing the evolution of the mole fractions of trimer, tetramer, and pentamer and of the sum of these chains in the R-0.7 sample.

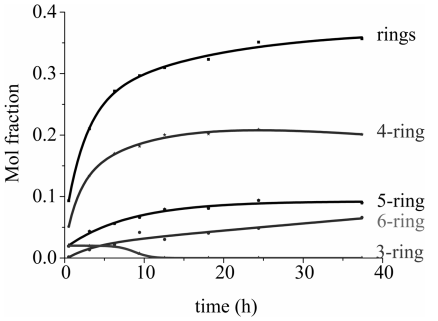

Figure 9. Detail of Figure 7 showing the evolution of the mole fractions of cyclic oligomers and of the sum of these ring structures in the R-0.7 sample.

cyclic species. Relative concentrations of oligomers were quantified based on the respective NMR signals divided by the number of silicon atoms in the respective species. Both nonhydrolyzed and hydrolyzed silicate groups were included in the estimation. The obtained distribution (Figure 7) is only an approximation due to the emerging presence of Q^3 silicon. Q^3 signals of differently sized branched rings coincided. Within the branched chain population, the Q^3 signal of differently sized chains overlapped as well. Therefore, branching could only be expressed as the content of Q^3 silicons in the totality of Si atoms (Figure 7). The distribution of the differently sized chains and rings is shown in Figure 8 and 9, respectively. In the R-0.7 sample, monomers were fully converted after 5−10 h. Dimers were the primary reaction product, but also some trimers and tetramers were formed by monomer addition. Dimers were consumed more slowly than monomers and persisted over the entire 40 h investigation period. Generally, at all times the formation of chains was favored over rings. Among the cyclic structures, especially the 3-rings were formed in very small quantities, presumably due to limited stability.[77] During the 40 h observation period, chains continued to grow up to tetramer and pentamer, even after monomer depletion. This now suggested chain growth via couplings of dimers or of dimer with trimer, respectively. Within 40 h, R-0.7 reached a silicon condensation degree of ∼45%, as determined by eq 2.

A key question was how the differently sized rings were formed. Possible scenarios included cyclization of chains or cyclodimerization. Qualitative insight into these mechanisms was gained from the derived quantitative distributions of oligomers (Figures 7−9). In the period 10−40 h, the concentration of 4-rings remained almost constant, while in the same period a steady increase of the tetrameric chain population occurred. This evolution was a clear argument against cyclization of a linear tetramer as the dominant mechanism of 4-ring formation. Similar arguments applied for the formation of 5-rings from dimer and trimer, rather than through cyclization. A further argument was the detection of 6-rings, while no linear hexamers ever reached the ^{29}Si NMR detection limit. An instantaneous cyclization of linear hexamers upon their formation appears unlikely because the linear tetramer and pentamer did not show any significant disposition to close. Formation of 6-rings through dimerization of a linear trimer and/or addition of dimer to tetramer seemed more likely. Inspection of the decrease of trimer concentration indeed fully confirmed this assumption (see Figure 5 in Supporting Information). A direct correlation between the consumption of silicon atoms in trimers with the formation of pentamer, 5-ring, and 6-ring clearly supported the hypothesis cyclodimerization was the dominant mechanism for ring formation. Furthermore, the excellent agreement between consumed and formed species also indicated 6-rings mostly are formed from two trimers rather than by addition of dimer and tetramer.

The UV−Raman spectra of R-0.7 (Figure 5) revealed the depletion of monomers and continuous decrease in dimers as observed with ^{29}Si NMR. The Raman signal of 4-rings emerged after 4 h and also remained present throughout the polymerization. This corresponded in time with the largest growth of 4-rings observed in the oligomer distribution with ^{29}Si NMR. In time, all vibrations broadened to a certain extent as their degree of branching increased. The additional contribution of the small populations of 5- and 6-rings was also reflected in the broadened nature of the ring vibration region. The Raman sequence was, like before, in full agreement with the sequence observed in more detail by ^{29}Si NMR.

The oligomerization steps which eventually led to the final silica gel were probed through the analysis of the evolution of the oligomer populations of R-1.2 from ^{29}Si NMR (see Figure 3 of Supporting Information). The sequence of appearing and consumed oligomers in R-1.2 was directly comparable to R-0.7 (see Figure 6 of Supporting Information). After conversion of all monomers by dimerization and chain growth, the dimer and trimer engaged the first 5 h in chain extension and cyclodimerization. Afterward they participated mainly in branching. At the end of the observation period, the system reached a silicon condensation degree of ∼55%, as determined by eq 2.

This was fully mirrored in the Raman sequence of the R-1.2 (see Figure 7 in Supporting Information). The intensity of the dimer signal decreased gradually, while the 4-ring signal gained intensity. Around 20 h, the tetramer became dominant over the trimer. In later stages, all Raman signals broadened. The only remainders represent end groups and a highly branched silicate population which ultimately led to gel formation.

The oligomerization scheme starting from TEOS at a low molar hydrolysis ratio in acidic media derived from ^{29}Si NMR and UV−Raman spectroscopy on R-0.2 to R-1.2 and even up to samples with *r*-values of 2.0 could be summarized as follows (Scheme 1). Monomer essentially served chain extension up to a linear tetramer. The formation of rings and branchings was slower but, like all observed processes, was accelerated by a higher molar hydrolysis ratio or heating. The formation of rings and of branching of rings and chains proceeded mainly from the dimer and trimer. Chain and ring size did not exceed 6 silicate units to which side chains of two and three additional silicate

Scheme 1. Oligomerization Scheme of TEOS in an Acid Medium and Substoichiometric Quantities of Water[a]

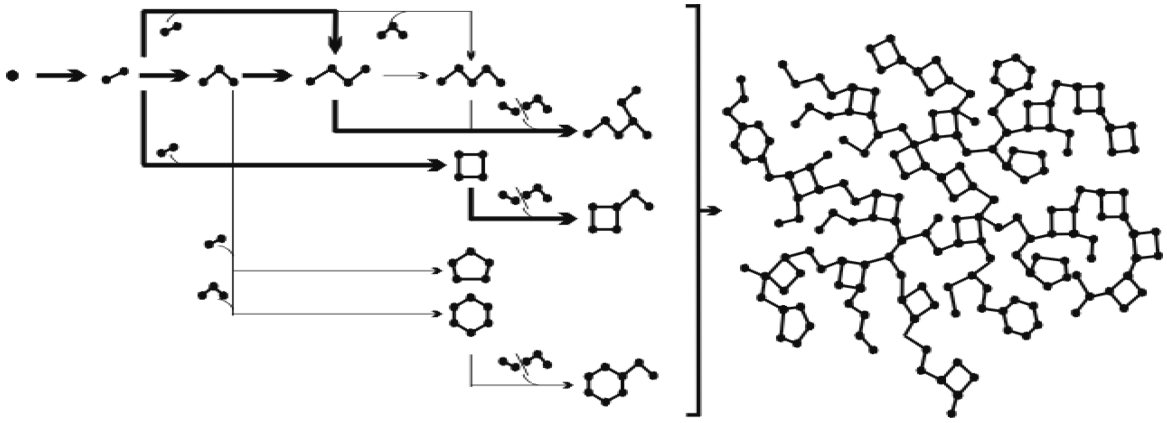

[a] The significance of a reaction pathway is revealed by the thickness of the arrow.

units were attached. The dominant rings were 4-rings. Gel presumably was formed through polycondensation of these branched molecules. The presumed nature of the gel network (Scheme 1) was found in agreement with the proposal by Kelts and Armstrong for silicate polymer growth from TEOS at low pH. They suggested formation of a tightly packed polymer, composed of interlinked 4-rings and short chains.[59]

CONCLUSIONS

The silicate oligomer chemistry in an acid-catalyzed silica sol−gel process departing from TEOS was analyzed using ^{29}Si NMR and UV−Raman spectroscopy in combination with molecular modeling. The formation of linear chains up to hexamer, rings composed of 3−6 Si atoms, and branched specimen was revealed based on spectroscopic signatures. Raman signals of the tetramer and rings with 4−6 Si atoms were observed and assigned relying on ^{29}Si NMR and molecular modeling.

The reaction scheme of acid-catalyzed silica sol−gel using TEOS and substoichiometric quantities of water was established (Scheme 1), and experimental evidence indicated this mechanism to be of general validity. The main reaction pathways were chain extensions of dimer through monomer addition, formation of rings via cyclodimerization, and branching through attachment of dimer and trimer. Secondary pathways were chain-formation through end-on dimerization of the dimer and trimer. The oligomerization process evolved toward a mixture of silicate species with short chains up to 4 Si atoms and 4-rings, both with the option to contain side chains of 2−4 Si atoms. Oligomers barely grew larger than 6−9 Si atoms. The polycondensation of this oligomer mixture was presumed to be responsible for gelation. This network was observed at molar hydrolysis ratios of 0.2−1.2, up to 2, and with hydrochloric or sulfuric acid. The present insight into the chemical nature of precursor oligomers will be helpful in the tuning of the synthesis of amorphous microporous silica materials.

ASSOCIATED CONTENT

Supporting Information. Full XYZ coordinates of all optimized structures for the molecular modeling of Raman intensities, Raman frequencies, and ^{29}Si NMR chemical shifts. The kinetic model for the initial steps of the condensation reactions. Characterization data (NMR spectra, evolutions of the mol fractions, Raman spectra). Complete ref 67. This material is available free of charge via the Internet at http://pubs.acs.org.

AUTHOR INFORMATION

Corresponding Author

*E-mail: johan.martens@biw.kuleuven.be.

ACKNOWLEDGMENT

A.D. and D.L. acknowledge the Research Foundation Flanders (FWO) for a research fellowship. Theoretical work was supported by the Research Board of Ghent University (BOF) and BELSPO, for supporting Interuniversity Attraction Poles (IAP-PAI P6/27). We greatly acknowledge Prof. Tatjana Parac-Vogt and Karel Duerinckx for ^{29}Si NMR measurements on a Bruker Avance II^{+} 600 spectrometer (Center for Molecular Design and Synthesis at K.U. Leuven, Belgium). J.A.M and C.E.A.K. acknowledge the Flemish Government for long-term structural funding (Methusalem), the Belgian Prodex office, and ESA.

REFERENCES

(1) Rouse, J. H.; Ferguson, G. S. *J. Am. Chem. Soc.* **2003**, *125*, 15529–15536.
(2) Shin, J. H.; Metzger, S. K.; Schoenfisch, M. H. *J. Am. Chem. Soc.* **2007**, *129*, 4612–4619.
(3) Uemura, T.; Hiramatsu, D.; Yoshida, K.; Isoda, S.; Kitagawa, S. *J. Am. Chem. Soc.* **2008**, *130*, 9216–9217.
(4) Wang, J.; Pamidi, P. V. A.; Zanette, D. R. *J. Am. Chem. Soc.* **1998**, *120*, 5852–5853.
(5) Colomban, P. *J. Raman Spectrosc.* **1996**, *27*, 747–758.
(6) James, P. F. *J. Non-Cryst. Solids* **1988**, *100*, 93–114.
(7) Bertoluzza, A.; Fagnano, C.; Antonietta Morelli, M.; Gottardi, V.; Guglielmi, M. *J. Non-Cryst. Solids* **1982**, *48*, 117–128.
(8) Brinker, C.; Scherer, G. *Sol-Gel Science: The Physics and Chemistry of Sol-Gel Processing*, Academic: New York, N. Y. 1990.
(9) Lin, C. C.; Basil, J. D. *Mater. Res. Soc. Symp. Proc.* **1986**, *73*, 585–90.
(10) Pouxviel, J. C.; Boilot, J. P.; Beloeil, J. C.; Lallemand, J. Y. *J. Non-Cryst. Solids* **1987**, *89*, 345–360.
(11) Assink, R. A.; Kay, B. D. *J. Non-Cryst. Solids* **1988**, *99*, 359–370.
(12) Bernards, T. N. M.; Vanbommel, M. J.; Boonstra, A. H. *J. Non-Cryst. Solids* **1991**, *134*, 1–13.
(13) Matsuyama, I.; Satoh, S.; Katsumoto, M.; Susa, K. *J. Non-Cryst. Solids* **1991**, *135*, 22–28.

(14) Mulder, C. A. M.; Damen, A. *J. Non-Cryst. Solids* **1987**, *93*, 169–178.
(15) Brinker, C. J.; Keefer, K. D.; Schaefer, D. W.; Ashley, C. S. *J. Non-Cryst. Solids* **1982**, *48*, 47–64.
(16) Brinker, C. J. *J. Non-Cryst. Solids* **1988**, *100*, 31–50.
(17) Aelion, R.; Loebel, A.; Eirich, F. *J. Am. Chem. Soc.* **1950**, *72*, 5705–5712.
(18) Assink, R. A.; Kay, B. D. *J. Non-Cryst. Solids* **1988**, *107*, 35–40.
(19) Gnado, J.; Dhamelincourt, P.; Pelegris, C.; Traisnel, M.; Mayot, A. L. *J. Non-Cryst. Solids* **1996**, *208*, 247–258.
(20) Lippert, J. L.; Melpolder, S. B.; Kelts, L. M. *J. Non-Cryst. Solids* **1988**, *104*, 139–147.
(21) Marino, I.-G.; Lottici, P. P.; Bersani, D.; Raschellà, R.; Lorenzi, A.; Montenero, A. *J. Non-Cryst. Solids* **2005**, *351*, 495–498.
(22) Matos, M. C.; Ilharco, L. M.; Almeida, R. M. *J. Non-Cryst. Solids* **1992**, *147−148*, 232–237.
(23) Ng, L. V.; Thompson, P.; Sanchez, J.; Macosko, C. W.; McCormick, A. V. *Macromolecules* **1995**, *28*, 6471–6476.
(24) Sassi, Z.; Bureau, J. C.; Bakkali, A. *Vib. Spectrosc.* **2002**, *28*, 299–318.
(25) Zerda, T. W.; Artaki, I.; Jonas, J. *J. Non-Cryst. Solids* **1986**, *81*, 365–379.
(26) Cho, H.; Felmy, A. R.; Craciun, R.; Keenum, J. P.; Shah, N.; Dixon, D. A. *J. Am. Chem. Soc.* **2006**, *128*, 2324–2335.
(27) Loy, D. A.; Carpenter, J. P.; Alam, T. M.; Shaltout, R.; Dorhout, P. K.; Greaves, J.; Small, J. H.; Shea, K. J. *J. Am. Chem. Soc.* **1999**, *121*, 5413–5425.
(28) Haouas, M.; Taulelle, F. *J. Phys. Chem. B* **2006**, *110*, 3007–3014.
(29) Artaki, I.; Bradley, M.; Zerda, T. W.; Jonas, J. *J. Phys. Chem.* **1985**, *89*, 4399–4404.
(30) Zerda, T. W.; Hoang, G. *J. Non-Cryst. Solids* **1989**, *109*, 9–17.
(31) Mora-Fonz, M. J.; Catlow, C. R. A.; Lewis, D. W. *J. Phys. Chem. C* **2007**, *111*, 18155–18158.
(32) Trinh, T. T.; Jansen, A. P. J.; van Santen, R. A.; Meijer, E. J. *Phys. Chem. Chem. Phys.* **2009**, *11*, 5092–5099.
(33) Fan, F. T.; Feng, Z. C.; Li, G. N.; Sun, K. J.; Ying, P. F.; Li, C. *Chem.−Eur. J.* **2008**, *14*, 5125–5129.
(34) Fotovat, F.; Kazemian, H.; Kazemeini, M. *Mater. Res. Bull.* **2009**, 913–17.
(35) Li, J.; Xiong, G.; Feng, Z.; Liu, Z.; Xin, Q.; Li, C. *Microporous Mesoporous Mater.* **2000**, *39*, 275–280.
(36) Xiong, G.; Yu, Y.; Feng, Z.-c.; Xin, Q.; Xiao, F.-S.; Li, C. *Microporous Mesoporous Mater.* **2001**, *42*, 317–323.
(37) Yu, Y.; Xiong, G.; Li, C.; Xiao, F.-S. *J. Catal.* **2000**, *194*, 487–490.
(38) Yu, Y.; Xiong, G.; Li, C.; Xiao, F.-S. *Microporous Mesoporous Mater.* **2001**, *46*, 23–34.
(39) Dutta, P. K.; Shieh, D. C.; Puri, M. *Zeolites* **1988**, *8*, 306–309.
(40) Knops-Gerrits, P.-P.; De Vos, D. E.; Feijen, E. J. P.; Jacobs, P. A. *Microporous Mater.* **1997**, *8*, 3–17.
(41) Dutta, P. K.; Rao, K. M.; Park, J. Y. *J. Phys. Chem.* **1991**, *95*, 6654–6.
(42) De Man, A. J. M.; Van Santen, R. A. *Zeolites* **1992**, *12*, 269–79.
(43) Knight, C. L.; Williamson, M. A.; Bodnar, R. J. *Microbeam Anal. (San Francisco)* **1989**, *24*, 571–3.
(44) Bornhauser, P.; Bougeard, D. *J. Raman Spectrosc.* **2001**, *32*, 279–285.
(45) Mozgawa, W. *J. Mol. Struct.* **2001**, *596*, 129–137.
(46) Dutta, P. K.; Del Barco, B. *J. Phys. Chem.* **1985**, *89*, 1861–5.
(47) Dutta, P. K.; Del Barco, B. *J. Phys. Chem.* **1988**, *92*, 354–7.
(48) Dutta, P. K.; Twu, J. *J. Phys. Chem.* **1991**, *95*, 2498–501.
(49) Bremard, C.; Le Maire, M. *J. Phys. Chem.* **1993**, *97*, 9695–702.
(50) Mozgawa, W.; Bajda, T. *J. Mol. Struct.* **2006**, *792−793*, 170–175.
(51) Mozgawa, W.; Jastrzebski, W.; Handke, M. *J. Mol. Struct.* **2006**, *792−793*, 163–169.
(52) Krause, K.; Geidel, E.; Kindler, J.; Förster, H.; Smirnov, K. S. *Vib. Spectrosc.* **1996**, *12*, 45–52.
(53) Pavel, C. C.; Zibrowius, B.; Loffler, E.; Schmidt, W. *Phys. Chem. Chem. Phys.* **2007**, *9*, 3440–3446.
(54) Dutta, P. K.; Shieh, D. C. *J. Phys. Chem.* **1986**, *90*, 2331–4.
(55) Dutta, P. K.; Shieh, D. C.; Puri, M. *J. Phys. Chem.* **1987**, *91*, 2332–6.
(56) Fan, F. T.; Sun, K. J.; Feng, Z. C.; Xia, H. A.; Han, B.; Lian, Y. X.; Ying, P. L.; Li, C. *Chem.−Eur. J.* **2009**, *15*, 3268–3276.
(57) Bailey, J. K.; Macosko, C. W.; Mecartney, M. L. *J. Non-Cryst. Solids* **1990**, *125*, 208–223.
(58) Brus, J.; Karhan, J.; Kotlik, P. *Collect. Czech. Chem. Commun.* **1996**, *61*, 691–703.
(59) Kelts, L. W.; Armstrong, N. J. *J. Mater. Res.* **1989**, *4*, 423–433.
(60) Maier, W. F.; Tilgner, I. C.; Wiedorn, M.; Ko, H. C. *Adv. Mater.* **1993**, *5*, 726–730.
(61) Aerts, C. A.; Verraedt, E.; Mellaerts, R.; Depla, A.; Augustijns, P.; Van Humbeeck, J.; Van den Mooter, G.; Martens, J. A. *J. Phys. Chem. C* **2007**, *111*, 13404–13409.
(62) Verraedt, E.; Pendela, M.; Adams, E.; Hoogmartens, J.; Martens, J. A. *J. Controlled Release* **2010**, *142*, 47–52.
(63) Depla, A.; Kirschhock, C.; Martens, J. In *Studies in Surface Science and Catalysis*; Gaigneaux, E. M., Devillers, M., Hermans, S., Jacobs, P. A., Martens, J. A., Ruiz, P., Eds.; Elsevier: New York, 2010; Vol. 175, pp 801−804.
(64) Aerts, C. A.; Verraedt, E.; Depla, A.; Follens, L.; Froyen, L.; Van Humbeeck, J.; Augustijns, P.; Van den Mooter, G.; Mellaerts, R.; Martens, J. A. *Int. J. Pharm.* **2010**, *397*, 84–91.
(65) Lazzeri, M.; Mauri, F. *Phys. Rev. Lett.* **2003**, *90*, 036401/1–036401/4.
(66) Casanovas, J.; Illas, F.; Pacchioni, G. *Chem. Phys. Lett.* **2000**, *326*, 523–529.
(67) Frisch, M. J. et al. *Gaussian 03*; Gaussian, Inc.: Wallingford, CT, 2003 (see complete ref 67 in Supporting Information).
(68) Lesthaeghe, D.; Vansteenkiste, P.; Verstraelen, T.; Ghysels, A.; Kirschhock, C. E. A.; Martens, J. A.; Van Speybroeck, V.; Waroquier, M. *J. Phys. Chem. C* **2008**, *112*, 9186–9191.
(69) Becke, A. D. *J. Chem. Phys.* **1993**, *98*, 5648–5652.
(70) Trinh, T. T.; Jansen, A. P. J.; van Santen, R. A. *J. Phys. Chem. B* **2006**, *110*, 23099–23106.
(71) Merrick, J. P.; Moran, D.; Radom, L. *J. Phys. Chem. A* **2007**, *111*, 11683–11700.
(72) Yu, Y.; Xiong, G.; Li, C.; Xiao, F. S. *Microporous Mesoporous Mater.* **2001**, *46*, 23–34.
(73) Mondragón, M. A.; Castaño, V. M.; J. Garcia, M.; C.A.; Téllez, S. *Vib. Spectrosc.* **1995**, *9*, 293–304.
(74) Devreux, F.; Boilot, J. P.; Chaput, F.; Lecomte, A. *Phys. Rev. A* **1990**, *41*, 6901.
(75) Trinh, T. T.; Jansen, A. P. J.; van Santen, R. A.; Meijer, E. J. *J. Phys. Chem. C* **2009**, *113*, 2647–2652.
(76) Trinh, T. T.; Jansen, A. P. J.; van Santen, R. A.; Vande Vondele, J.; Meijer, E. J. *ChemPhysChem* **2009**, *10*, 1775–1782.
(77) Harris, R. K.; Knight, C. T. G. *J. Chem. Soc., Faraday Trans. 2: Mol. Chem. Phys.* **1983**, *79*, 1525–38.